Journal of Solid State Chemistry **153,** 16–25 (2000)
doi:10.1006/jssc.2000.8712, available online at http://www.idealibrary.com on IDEAL®

Systematic Structural Change in Selected Rare Earth Oxide Pyrochlores as Determined by Wide-Angle CBED and a Comparison with the Results of Atomistic Computer Simulation

Yasunori Tabira[1] and Ray L. Withers

Research School of Chemistry, Australian National University, Canberra, ACT 0200, Australia

and

Licia Minervini and Robin W. Grimes

Department of Materials, Imperial College, Prince Consort Road, London, SW7 2BP, United Kingdom

Received December 8, 1999; in revised form February 29, 2000; accepted March 10, 2000; published online June 26, 2000

An unknown oxygen atom fractional co-ordinate characteristic of the pyrochlore structure type has been determined for selected rare earth zirconate and titanate pyrochlores via a systematic row wide-angle CBED technique and shown to vary systematically with rare earth ion size. In the case of the titanate pyrochlore $Gd_2Ti_2O_7$, the obtained results contrast with previously published X-ray results. Atomistic computer simulation is used to predict the value of the same parameter for a wide range of oxide pyrochlores. Comparison of calculated values with experimentally determined values shows that the general trends are correctly predicted although there appears to be systematic underestimation of both the observed values (by approximately 0.007) as well as their rate of change with rare earth ion size. Cation anti-site disorder is proposed as the origin of these discrepancies.

1. INTRODUCTION

Rare earth oxide pyrochlores, of ideal stoichiometry $R_2M_2(O1)_6(O2)_1$, crystallize in space group $Fd3m$ (origin choice 2) with four crystallographically independent atom sites (R^{3+}, a rare earth ion, in 16*d* at $\frac{1}{2}, \frac{1}{2}, \frac{1}{2}$, M^{4+} in 16*c* at 000, O1 in 48*f* at $x, \frac{1}{8}, \frac{1}{8}$, and O2 in 8*b* at $\frac{3}{8}, \frac{3}{8}, \frac{3}{8}$). The structure type can be considered as an ordered defect fluorite structure with the trivalent rare earth R^{3+} and quadrivalent M^{4+} cations forming an ordered, *ccp* eutectic cation array, into $\frac{7}{8}$, of the tetrahedral interstices of which are located the oxygen ions: O1 in an off-center position within the R_2M_2 tetrahedra, O2 in the R_4 tetrahedra and with the M_4 tetrahedra remaining empty (1, 2; see Fig. 1). For a regular octahedral oxygen environment around the quadrivalent M^{4+} cations, x should be 0.3125, whereas, for a regular cubic oxygen environment around the large trivalent rare earth ion, x should be 0.375. (Note that in a previous paper (3) a different but equivalent position for the 48*f* oxygen ion, $\frac{1}{4} - x, \frac{1}{8}, \frac{1}{8}$, was used.)

The exact value of x could be expected to be sensitively dependent upon the absolute sizes, and size differences between, the constituent rare earth, R^{3+}, and quadrivalent, M^{4+}, cations and provides a good test for atomistic simulation techniques (4–6) to bench mark themselves against. In this paper, the value of x is determined for selected rare earth zirconate and titanate pyrochlores via a systematic row wide-angle CBED technique and compared with the results of atomistic simulation.

Rare earth zirconate pyrochlores are known to exist for R = La to Gd (1, 2), but to date very little has been reported with respect to the corresponding values of x (3). Rare earth titanate pyrochlores exist for R = Sm to Lu (1, 2, 7) but, according to previously reported X-ray structure refinement results (7), the value of x does not change systematically with rare earth ion (see Fig. 2). On ionic size of grounds alone, one might expect the value of x to change monotonically as the ionic size of the relevant rare earth ions shrink relative to the size of the same quadrivalent M^{4+} cation within the one $R_2M_2O_7$ family of oxide pyrochlores (see, for example, the recently reported results for stannate pyrochlores (8)). Given the difficulty in refining the value of x from X-ray diffraction data as a result of the low relative scattering power of the light oxygen atoms, it was thought worthwhile to re-determine the value of x for selected titanate pyrochlores using CBED.

[1] To whom correspondence should be addressed.

0022-4596/00 $35.00

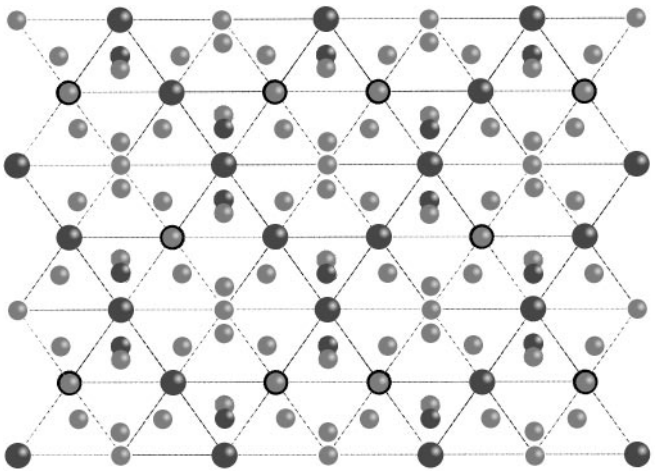

FIG. 1. The ideal pyrochlore structure shown in projection along ⟨110⟩. The lines connecting the metal ions forming the ccp cation array (light M^{4+}, dark R^{4+}) are shown. The O1 oxygen ions (light) are at off-center positions in the R_2M_2 tetrahedra, while the O2 ions (dark) are at the center of the R_4 tetrahedra.

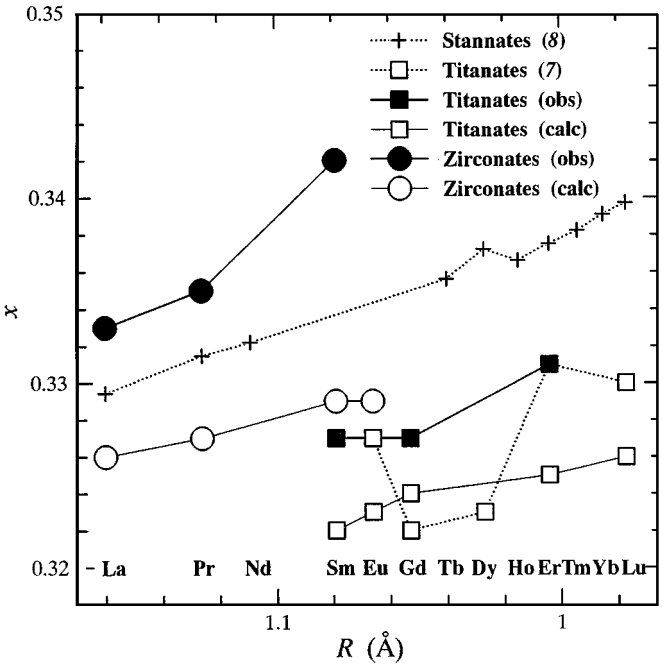

FIG. 2. WACBED-determined x parameters (dark symbols) plotted as a function of the ionic radii R^{3+} of the relevant rare earth species for the zirconate and titanate pyrochlores studied in the present work. The open squares represent the previously reported, X-ray determined values in the case of the titanate pyrochlores.

2. EXPERIMENTAL PROCEDURES

Synthesis

The rare earth oxide, La_2O_3, Pr_2O_3, Sm_2O_3, Er_2O_3 (Research Organic/Inorganic Chemical Corp., 99.9%), Gd_2O_3 (Halewood Chemicals, Ltd., 99.9%), TiO_2 (Aldrich Chemical Company, Inc., 99.99%), and ZrO_2 (Z—Tech, $>99.9\%$, including 2.57% HfO_2), starting materials were fired at 1000°C for a day before weighing. (The nominal rare earth sesquioxides were found to be extremely hygroscopic, so pre-firing before weighing was found to be essential (3, 9).) The resultant component oxides, made up to the stoichiometry $R_2M_2O_7$, were then thoroughly mixed mechanically with ethanol before being pressed into pellets. The pellets were placed on alumina tiles and heated at 1500°C for 3 days followed by re-pelleting before heating again at 1500°C for a further 3 days. Platinum supports and vessels were avoided due to the reaction of platinum with the lighter rare earth element containing specimens. The pellets were subsequently quenched in air from 1500°C.

XRD patterns using a Guinier–Hägg camera (monochromated Cu$K\alpha_1$ radiation, 25 mA × 40 kV) confirmed that the appropriate pyrochlore product was obtained and gave resultant pyrochlore unit cell dimensions $a_0 =$ 10.802(1) Å, 10.692(1) Å, 10.587(1) Å for $La_2Zr_2O_7$, $Pr_2Zr_2O_7$, $Sm_2Zr_2O_7$, and $a_0 = 10.231(1)$ Å, 10.182(1) Å and 10.074(1) Å for $Sm_2Ti_2O_7$, $Gd_2Ti_2O_7$, $Er_2Ti_2O_7$, respectively, in good agreement with previously reported results (1, 2). A plot of refined unit cell dimension against ionic radii of the relevant rare earth ions (10) (see Fig. 3) shows a good linear relationship.

WACBED

Specimens for electron microscopy were prepared by crushing and dispersing onto holey carbon-coated copper grids. Wide-angle CBED (WACBED) patterns of these crushed polycrystalline specimens were taken using a Philips EM430 electron microscope, operating at 300 kV. [111]* systematic row geometry was used, and the irradiated area on a crystal fragment was usually around 500 Å. Typically the 11, 11, 11 reflection was tilted close to the exact Bragg position in selected area diffraction mode before convergence of the incident beam orientation to give rise to the experimental WACBED pattern. The typical convergence angle of the incident beam around $g_{11,11,11}$ was $\sim 0.4°$ giving rise to reflections from $g = 777$ to 15,15,15 (just) being excited within the 11,11,11 CBED disc (see Fig. 4). For more details on the diffraction geometry employed see (3, 9).

Unsaturated ordinary film negatives were digitized by a scanner into 8-bit image depth using 600 dpi resolution. Line profiles perpendicular to the diffraction lines in Fig. 4 were obtained after averaging the intensity pixel by pixel along the diffraction lines. Typically each line profile was composed of about 300 data points. Then pixel units were transformed into k_x, the projection component of the incident k_0 onto the ZOLZ plane, in units of $|g_{111}|$, followed by

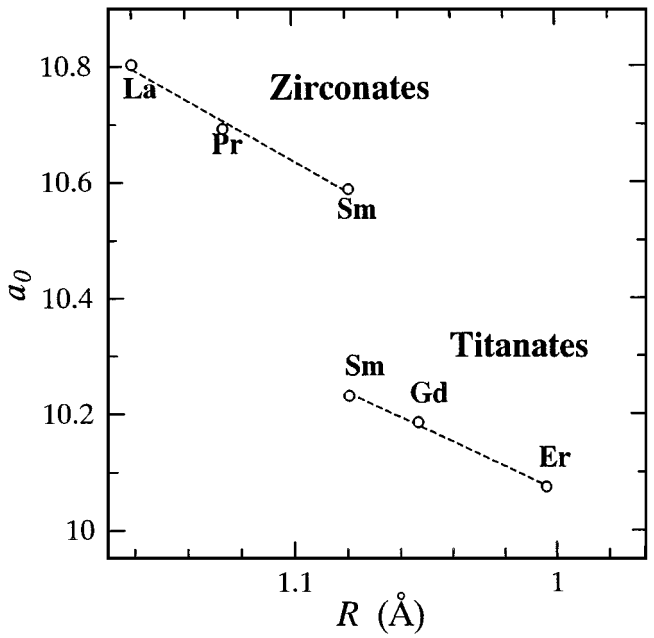

FIG. 3. Refined cell parameter a_0 of the $R_2^{3+}M_2^{4+}O_7$ pyrochlores ($M^{4+} = Zr^{4+}$, Ti^{4+}) as a function of the R^{3+} cation radius.

background subtraction using a polynomial function up to minus 4th order in k_x.

Specimen thickness was estimated from the diffraction width of the line profiles. A fully dynamical calculation utilizing the appropriate electron scattering factors (11) was carried out as a function of the inclination of the incident beam over orientations ranging from $k_x/g_{111} = 3.75$ up to 7.25 at intervals of 0.0125. Thirty-five beams from -8, -8, -8 up to 26, 26, 26 along the [111]* systematic row were included in the calculation. The thickness variation which inevitably exists to some extent in an illuminated area of crushed powder was taken into account by averaging the simulated line profiles for five different thicknesses up to $\pm 10\%$ around the appropriate average thickness. An average thickness of 150 nm, for example, would lead to calculated line profiles for 135, 142.5 150, 157.5, and 165 nm being summed up and averaged.

3. THEORETICAL DISCUSSION

Atomistic computer simulation techniques, based on energy minimization with a Born-like description of the lattice (4), were used to generate the pyrochlore structure. The procedures are based upon a description of lattice forces in terms of effective potentials. The perfect lattice is described by defining a cubic unit cell which is repeated throughout space using periodic boundary conditions as defined by the crystallographic lattice vectors. The total energy of the crystal is minimized by allowing the ions in the unit cell and the lattice vectors to relax to zero strain.

Interactions due to long-range Coulombic forces, summed using Ewald's method (12), as well as short-range

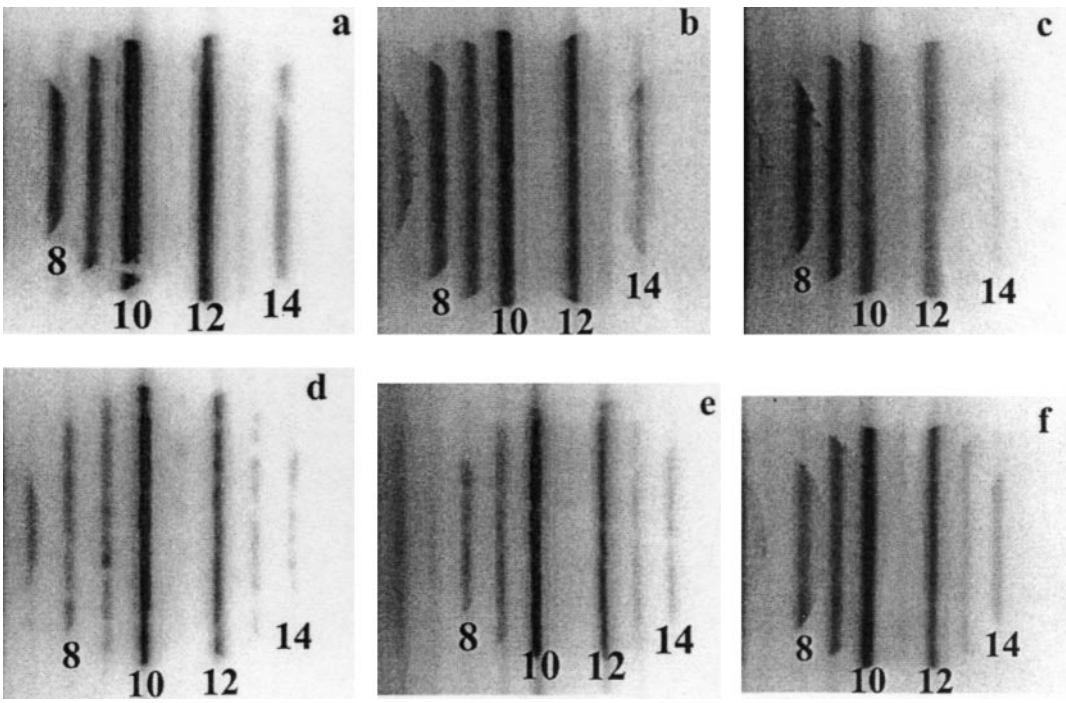

FIG. 4. Observed WACBED patterns from the relevant zirconates (a) $La_2Zr_2O_7$, (b) $Pr_2Zr_2O_7$, and (c) $Sm_2Zr_2O_7$ and titanates (d) $Sm_2Ti_2O_7$, (e) $Gd_2Ti_2O_7$, and (f) $Er_2Ti_2O_7$. The numbers shown below the diffraction lines are the order h of the corresponding hhh reflection. Note that the relative intensities of 888 and 999 to 10,10,10 systematically increase from (a) to (c), and (d) to (f), as the ionic size of the rare earth element decreases.

TABLE 1
Short-Range Potential Parameters

Species	A (eV)	ρ (Å)	C (eV Å^6)	Ref.
O^{2-}–O^{2-}	9547.96	0.2192	32.0	21
Lu^{3+}–O^{2-}	1618.80	0.33849	19.27	13
Yb^{3+}–O^{2-}	1649.80	0.3386	16.57	13
Er^{3+}–O^{2-}	1739.91	0.3389	17.55	13
Y^{3+}–O^{2-}	1766.40	0.33849	19.43	21
Gd^{3+}–O^{2-}	1885.75	0.3399	20.34	21
Eu^{3+}–O^{2-}	1925.71	0.3403	20.59	21
Sm^{3+}–O^{2-}	1944.44	0.3414	21.49	13
Nd^{3+}–O^{2-}	1995.20	0.3430	22.59	13
Pr^{3+}–O^{2-}	2086.01	0.3430	23.94	
La^{3+}–O^{2-}	2088.89	0.3460	23.25	21
Ti^{4+}–O^{2-}	2131.04	0.3038	0.0	13
Ru^{4+}–O^{2-}	1215.78	0.3441	0.0	13
Mo^{4+}–O^{2-}	1223.97	0.3470	0.0	13
Sn^{4+}–O^{2-}	1414.32	0.3479	13.66	13
Zr^{4+}–O^{2-}	1502.11	0.3477	5.1	13
Pb^{4+}–O^{2-}	1640.34	0.3507	19.50	13
Ce^{4+}–O^{2-}	1809.68	0.3547	20.40	21

forces, modeled using parameterized pair potentials, S_{ij}, were taken into consideration. The short-range term accounts for the electron cloud overlap and dispersion interactions (negligible beyond a few lattice spacings). In order to reduce computational time, short-range interactions were set to zero beyond 20 Å. In this study the Buckingham potential form was used,

$$S_{ij} = Ae^{(-r_{ij}/\rho)} - C/r_{ij}^6 \qquad [1]$$

where A, ρ, and C are three adjustable parameters (see Table 1). The values of the potential parameters were chosen so as to reproduce the known unit cell dimensions of a wide range of oxide pyrochlores while maintaining the same oxygen–oxygen potential (13).

The polarizability of the ions was accounted for via the shell model (14). This consists of a massless shell with charge $X|e|$ that is allowed to move with respect to a massive core of charge $Y|e|$; the overall charge state of each ion is therefore equal to $(X + Y)|e|$. The core and shell charges are connected by an isotropic harmonic spring force of constant k. Displacement of the shell relative to the core gives a good description of electronic polarization. In all calculations, O^{2-} and the larger 4 + cations (Zr, Pb, Ce) are treated as polarizable using the shell model: for O^{2-}, $Y = -2.04$, $k = 6.3$ eV Å^{-2}; Zr^{4+}, $Y = -0.05$, $k = 189.7$ eV Å^{-2}; Pb^{4+}, $Y = -0.05$, $k = 205.0$ eV Å^{-2}; Ce^{4+}, $Y = -0.20$, $k = 177.84$ eV Å^{-2}.

The type of calculation employed in this paper is usually referred to as "static" since lattice vibration entropy contributions are not included in the model. Furthermore configurational entropy is also ignored. The energies calculated are therefore enthalpies and relate, via the quasi-harmonic approximation, to the temperature of the lattice to which the potential parameters were fitted, in this case, room temperature. Entropy contributions are usually small at room temperature, but nevertheless this introduces some uncertainty. For further details of the computational methods used see (4–6). In all cases, calculations were carried out using the CASCADE code (15).

4. EXPERIMENTAL RESULTS

Figure 4 shows typical experimental WACBED patterns obtained for each synthesized pyrochlore: zirconates (a) $La_2Zr_2O_7$, (b) $Pr_2Zr_2O_7$, (c) $Sm_2Zr_2O_7$ and titanates (d) $Sm_2Ti_2O_7$, (e) $Gd_2Ti_2O_7$, (f) $Er_2Ti_2O_7$. The numbers shown underneath the respective diffraction lines correspond to the order h of the relevant hhh reflection. Note that the observed intensities of the 888, I_{888}, and 999, I_{999}, reflections relative to the intensity of the 10, 10, 10 reflection, $I_{10,10,10}$, are systematically smaller for the titanates than they are for the corresponding zirconates, which in turn requires that the x values for the titanates are smaller than those for the corresponding zirconates (cf. with Fig. 4 of (3)). Note further that I_{888} and I_{999} systematically grow relative to $I_{10,10,10}$ from (a) to (c), and from (d) to (f), as the ionic size of the rare earth element decreases. Qualitatively, this implies a systematic increase in x as the ionic size of the rare earth element decreases, as would be expected from a crystal chemical point of view.

The most significant difference between these experimental observations and what would be expected given the previously reported x values (in the case of the titanate pyrochlores (7) is that significant intensity, I_{999}, was genuinely observed in the WACBED line profile in the case of $Gd_2Ti_2O_7$ (see Fig. 4e). Figure 5 shows calculated WACBED line profiles in the case of $Gd_2Ti_2O_7$ (assuming $x = 0.322$ as reported in (1, 2, 7) for four different values of the associated isotropic temperature factors B, i.e., 0, 0.5, 1, 2 Å^2, for (a) Gd, (b) Ti, (c) O1, and (d) O2, respectively. The B factors for atoms other than the relevant atom in each of (a)–(d) were set to 0.5 Å^2 in each case. For more information as to the detailed dependence of WACBED line profiles on each B, see (3, 9). What is relevant here is that it was not possible via any practical combination of B factors to reproduce a 999 reflection with anywhere near enough intensity to be comparable with that observed experimentally (cf. Fig. 4e with Fig. 5). Since our previous studies of zirconate pyrochlores (3, 9) show that increasing x from 0.3125 toward that characteristic of the fluorite structure (0.375) makes I_{888} and I_{999} systematically increase relative to $I_{10,10,10}$, this implies that x itself must be larger than the previously reported value of 0.322.

Experimentally, the relative intensities of the observed reflections in the WACBED line profiles were found to be

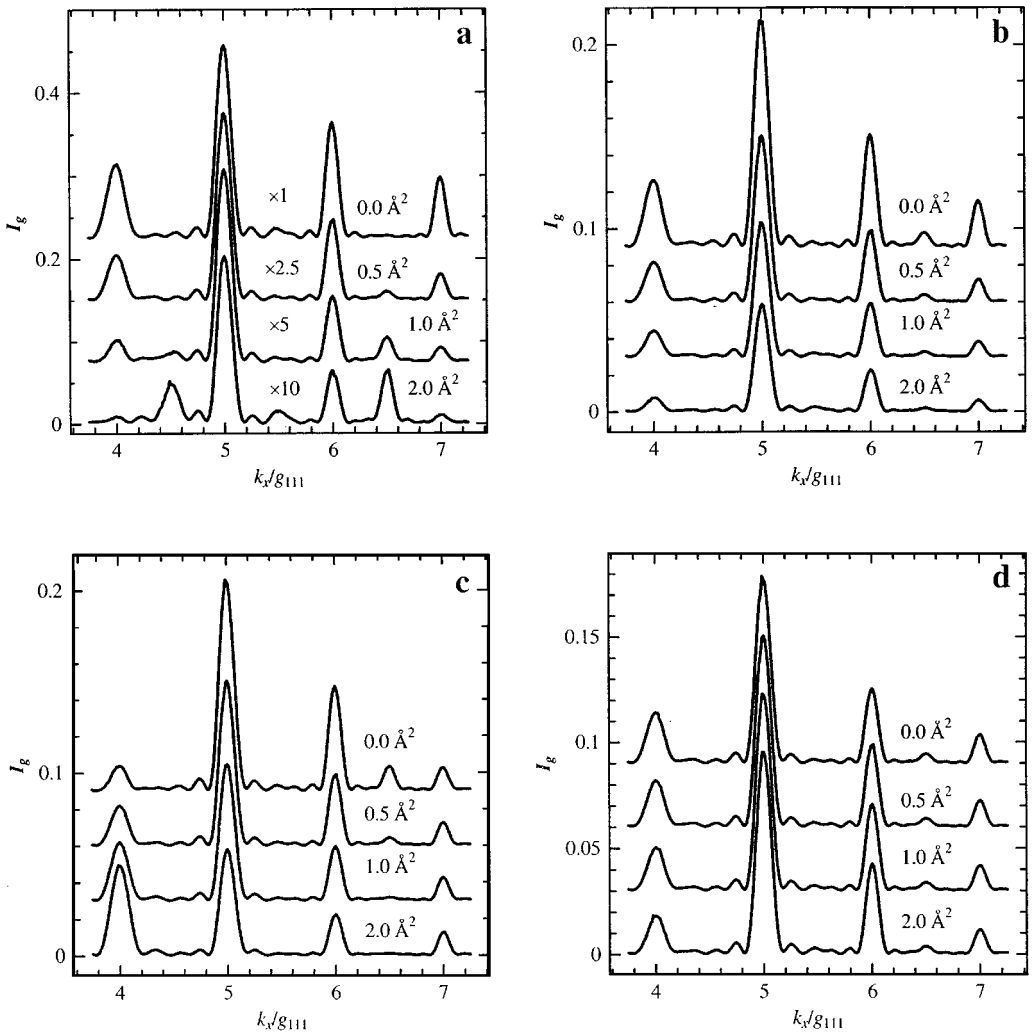

FIG. 5. Shows calculated WACBED line profiles in the case of $Gd_2Ti_2O_7$ (assuming the previous X-ray determined value for x of 0.322) for four different values of the associated isotropic temperature factors B, i.e., 0, 0.5, 1, 2 Å^2, for (a) Gd, (b) Ti, (c) O1, and (d) O2. The B factors for atoms other than the relevant atom in each of (a)–(d) were set to 0.5 Å^2 in each case.

not particularly sensitive to thickness. Nonetheless, given that the observed intensities are not kinematic (3, 9), it is important to check the quality of the quantitative fitting of calculated profiles to observed ones at more than one thickness. The best final fits (see Figs. 6 and 7 for the zirconates and the titanates, respectively) were obtained with the following structural parameters: $x = 0.333$, $B_{La} = \frac{3}{4}$, $B_{Zr} = \frac{1}{2}$, $B_{O1} = \frac{1}{4}$, $B_{O2} = \frac{1}{2}$ Å^2 for $La_2Zr_2O_7$; $x = 0.335$, $B_{Pr} = \frac{1}{2}$, $B_{Zr} = \frac{1}{2}$, $B_{O1} = \frac{1}{4}$, $B_{O2} = \frac{1}{2}$ Å^2 for $Pr_2Zr_2O_7$; $x = 0.342$, $B_{Sm} = \frac{3}{4}$, $B_{Zr} = \frac{1}{2}$, $B_{O1} = \frac{1}{4}$, $B_{O2} = \frac{1}{2}$ Å^2 for $Sm_2Zr_2O_7$; and $x = 0.327$, $B_{Sm} = 1$, $B_{Ti} = \frac{1}{2}$, $B_{O1} = \frac{3}{4}$, $B_{O2} = \frac{1}{2}$ Å^2 for $Sm_2Ti_2O_7$; $x = 0.327$, $B_{Gd} = 1$, $B_{Ti} = \frac{1}{2}$, $B_{O1} = \frac{3}{4}$, $B_{O2} = \frac{1}{2}$ Å^2 for $Gd_2Ti_2O_7$; and $x = 0.331$, $B_{Er} = 1$, $B_{Ti} = \frac{1}{2}$, $B_{O1} = \frac{1}{2}$, $B_{O2} = \frac{1}{2}$ Å^2 for $Er_2Ti_2O_7$. (The small difference in calculated x value for $La_2Zr_2O_7$ from that reported in (3) is due to the slightly more accurate method [as far as the number of contributions that are included given the known diffraction conditions] of summing up the individual rocking curves for each relevant reflection used in the current paper.)

The x values obtained in the present study are shown plotted against the ionic radii of the relevant rare earth ion (10) in Fig. 2. Those previously reported for the rare earth stannate pyrochlores in (8) are also shown in Fig. 2. The significant change in the previously reported x value for $Gd_2Ti_2O_7$ is apparent as is the systematic increase in x with decreasing rare earth ionic radii apparent in both titanate and zirconate pyrochlores along with the greater apparent sensitivity of the zirconate pyrochlores to rare earth ion size.

Figure 8 shows Bond Valence Sums (16–18), or Apparent Valences (AV's), for each of the constituent ionic species (calculated using the bond valence parameters of (16) as a

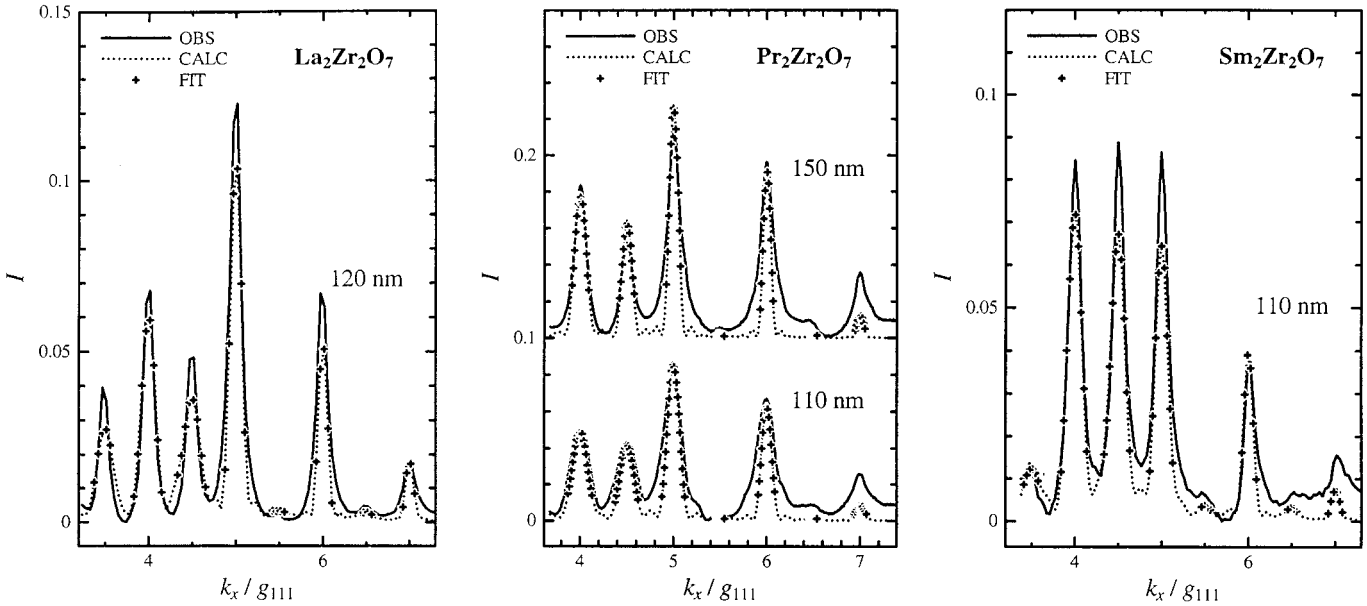

FIG. 6. Shows the best fit to the observed WACBED line profiles for the relevant zirconate pyrochlores.

function of x for the two extreme cases studied in each of the zirconate and titanate family of pyrochlores, i.e., for $La_2Zr_2O_7$ and $Sm_2Zr_2O_7$ in Fig. 8a and for $Sm_2Ti_2O_7$ and $Er_2Ti_2O_7$ in Fig. 8b. In both cases, the AV's of the rare earth ions increase while those of the quadrivalent ion decrease as x increases. In the case of the zirconate pyrochlores, AV calculations suggest a value for x of 0.330 for $La_2Zr_2O_7$ and 0.339 for $Sm_2Zr_2O_7$. (The corresponding WACBED-determined values were 0.333 and 0.342, respectively.) In the case of the titanate pyrochlores, such AV calculations suggest a value for x of 0.323 for $Sm_2Ti_2O_7$ and 0.332 for $Er_2Ti_2O_7$. (The corresponding WACBED-determined values were 0.327 for $Sm_2Ti_2O_7$ and 0.331 for $Er_2Ti_2O_7$.) Note that all of the observed x values (except for $Er_2Ti_2O_7$) are larger

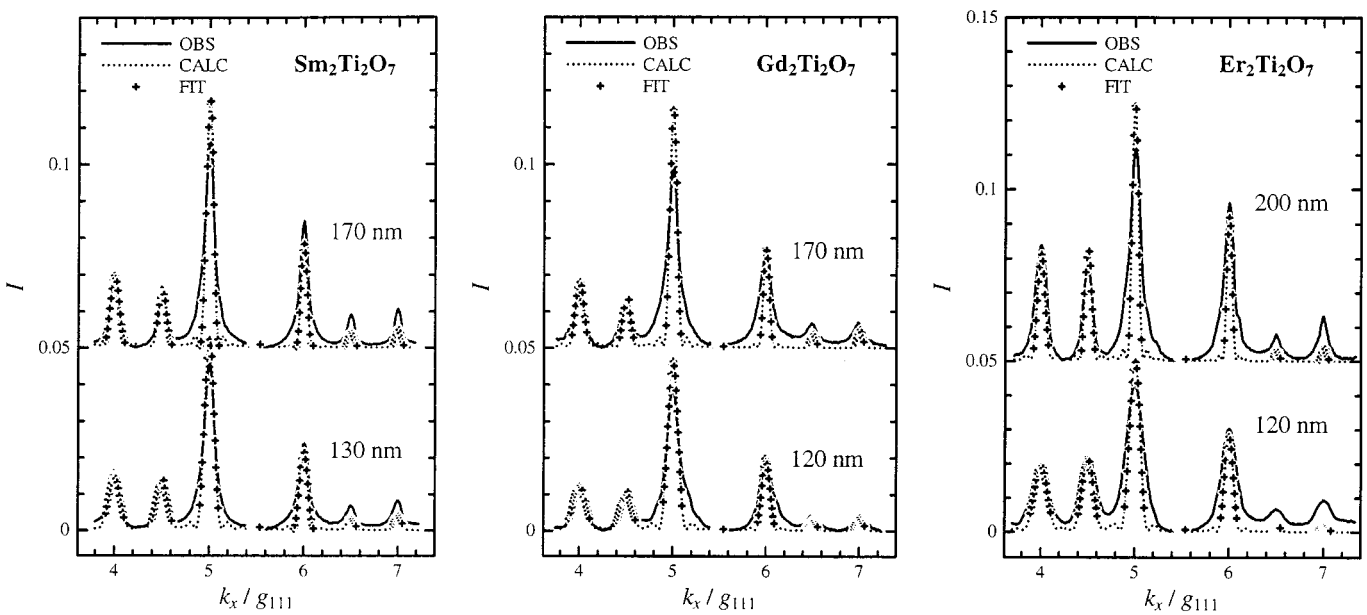

FIG. 7. Shows the best fit to the observed WACBED line profiles for the relevant titanate pyrochlores. WACBED fitting results were obtained for two significantly different thicknesses to make sure that the obtained results are thickness independent.

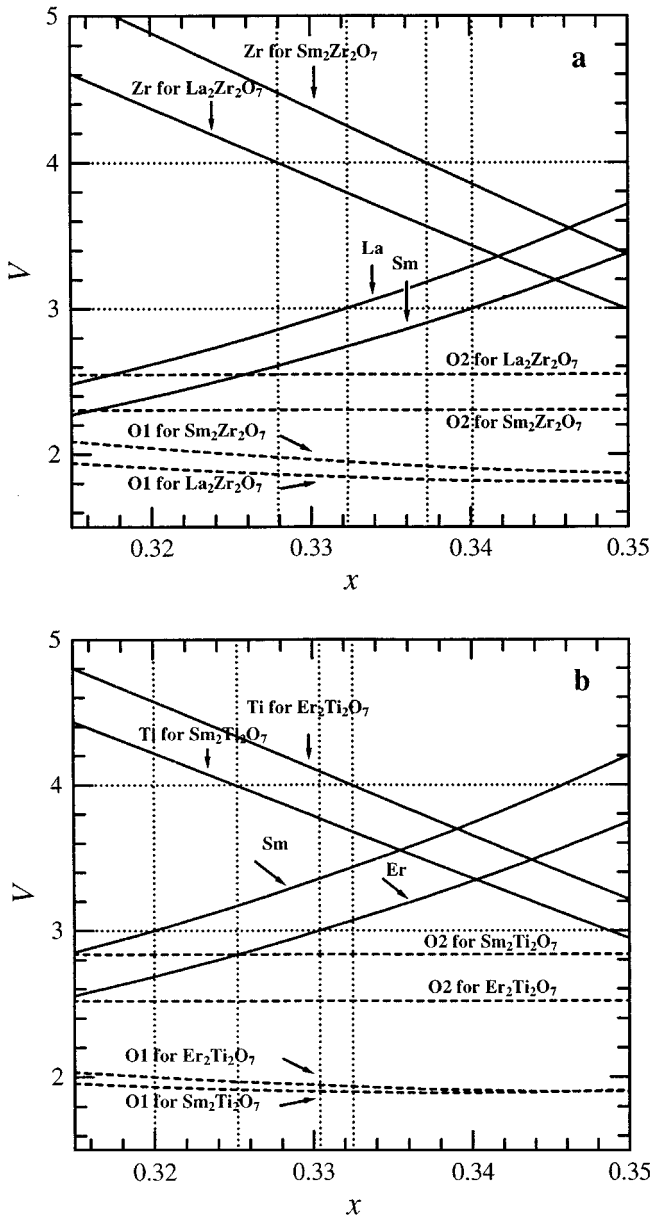

FIG. 8. Calculated apparent valences V of the constituent species in the (a) zirconate pyrochlores and (b) titanate pyrochlores as a function of the unknown fractional co-ordinate x of O1. Dotted lines show the formal V values of 3, 4 for R^{3+}, M^{4+} cations, respectively, and the corresponding expected x values.

than those predicted by the bond valence method. It is believed that this can be attributed to residual cation anti-site disorder (see below). AV calculations suggest that the effective charge transfer caused by such anti-site disorder will lead to increased values of x (9).

Finally, it is worthwhile noting that the same characteristic pattern of structured diffuse scattering (in the form of $\{110\}$* polarized sheets of diffuse intensity) recently reported as existing in the case of $La_2Zr_2O_7$ (19) also exists in the cases of each of the titanate and zirconate pyrochlores studied in the current contribution (see, for example, Fig. 9a–c for the titanate pyrochlores). The azimuthal intensity variation of this diffuse scattering shows that it is primarily

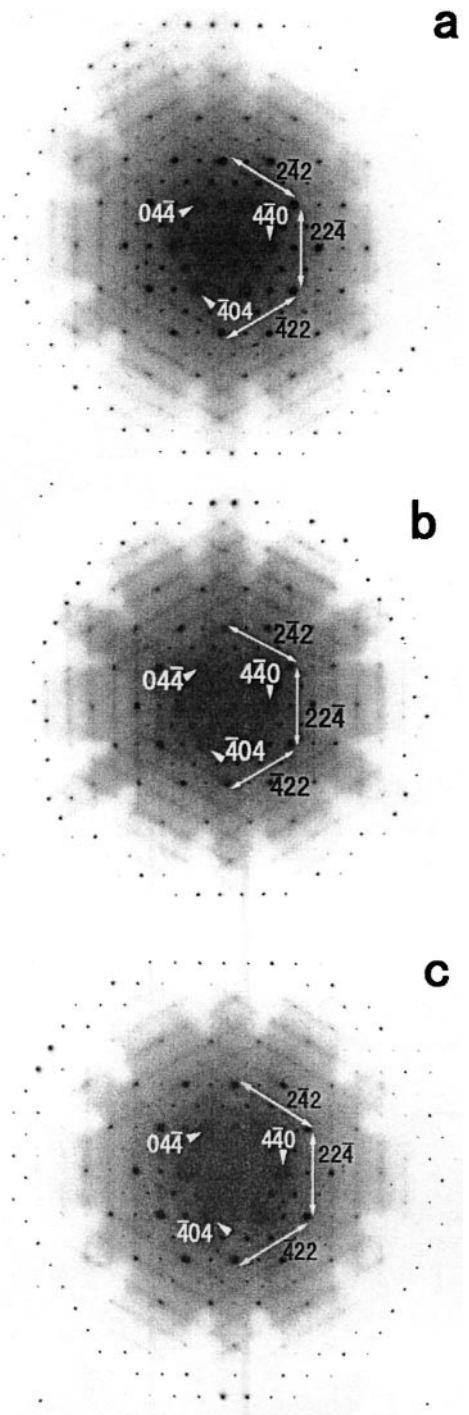

FIG. 9. Shows $\langle 111 \rangle$ zone axis EDP's of titanates, (a) $Sm_2Ti_2O_7$, (b) $Gd_2Ti_2O_7$, and (c) $Er_2Ti_2O_7$, characteristic of all the pyrochlore structures examined in this study and showing highly structured diffuse streaking along all directions perpendicular to the $\langle 110 \rangle$ directions of real space.

displacive in origin and related to correlated thermal vibration of essentially rigid $O(2)La_4$ tetrahedra rather than residual cation anti-site disorder (9).

5. THEORETICAL RESULTS

The predicted x values for a wide range of oxide pyrochlores calculated using the atomistic simulation techniques outlined in Section 3 above (assuming perfect cation ordering, i.e., no cation anti-site and associated disorder) are given in Table 2, compared with the experimental values obtained from this paper and the wider literature. Through this comparison, it becomes clear that, although the general trend is accurate, the predictions systematically underestimate the observed values by approximately 0.007 (see Table 2). The rate of change of x with rare earth ion size is also underestimated—at least for the stannate and zirconate pyrochlores although not so apparently for the titanate pyrochlores.

Figure 10 shows a contour map of the theoretically predicted oxygen positional parameter, x, as a function of the trivalent rare earth R and quadrivalent M cation radii. The thick white contour on the right side of Fig. 10 defines a boundary for the calculated stability of the ordered ternary compound with respect to the binary oxides:

$$A_2O_3 + 2BO_2 \leftrightarrow A_2B_2O_7 \qquad [2]$$

A negative reaction enthalpy indicates stability so that stable compounds lie to the left of the contour while unstable compounds lie to the right of this contour.

Pyrochlore compounds observed experimentally are shown as black circles. Pyrochlore compounds for which experimental data is not available but for which calculations have been carried out are shown as black crosses. White circles indicate compounds that have been synthesized by high pressure techniques (300 MPa, 700°C) (20). Noncubic $A_2B_2O_7$ compounds are shown as white crosses: in these cases, calculations predict the cubic phase to be stable with respect to the binary oxides, but experimentally a distortion from cubic symmetry is observed. Noncubic phases have not been thoroughly characterized crystallographically and hence calculations are performed assuming the higher cubic symmetry.

Figure 10 clearly predicts that x should increase with M^{4+} cation size for a given rare earth cation, in agreement with the larger values found for x in the case of the zirconate pyrochlores relative to those found for the titanate pyrochlores (see Fig. 2). This is because, as the M^{4+} cation decreases in size, the 48*f* oxygen ions will increasingly shift toward it. Conversely, for a given M^{4+} cation, x is predicted to decrease with rare earth R^{3+} cation size, also in general agreement with observation (see Fig. 2 and (8)). Now the presence of a large R^{3+} cation encourages the shift of the 48*f* oxygen ions toward the smaller M^{4+} cation. Neither of these effects is exactly linear with cation radius because of lattice relaxation effects. It is interesting to note that combinations of large M^{4+} cations and small R^{3+} cations are predicted to have large x values approaching those appropriate for a fluorite structure, and in fact solutions of Y_2O_3:$2CeO_2$, for example, form disordered fluorite solid solutions rather than ordered pyrochlore structures. On the other hand, combinations of small M^{4+} cations and large R^{3+} cations have smaller x values and form distorted pyrochlore structures. Thus the cubic pyrochlore structure is only stable within a relatively small range of x values

We believe that the reason for the systematic underestimation of x apparent in Table 2 is due to residual and unavoidable cation anti-site disorder which results in an associated structural relaxation (13). It has recently been shown, for example, that the value of x systematically increases with increasing cation anti-site disorder on either side of the nominally stoichiometric ($\varepsilon = 0.5$) composition in the wide-range nonstoichiometric $(1-\varepsilon)ZrO_2 \cdot \varepsilon SmO_{1.5}$ system (9). Indeed, the value of x was found to be 0.348 for $\varepsilon = 0.45$ or 0.55 (corresponding to $\sim 10\%$ cation anti-site

TABLE 2
Comparison of Experimental and Predicted Positional Parameter *x* of O1

Compound	Experiment	Predicted	Δ	Ref.
$Lu_2Ti_2O_7$	0.330	0.326	− 0.004	2
$Er_2Ti_2O_7$	0.331	0.325	− 0.006	This study
$Y_2Ti_2O_7$	0.328	0.325	− 0.003	2
$Gd_2Ti_2O_7$	0.327	0.324	− 0.003	This study
$Eu_2Ti_2O_7$	0.327	0.323	− 0.004	2
$Sm_2Ti_2O_7$	0.327	0.323	− 0.004	This study
$Y_2Ru_2O_7$	0.335	0.326	− 0.009	22
$Gd_2Ru_2O_7$	0.334	0.324	− 0.010	2
$Eu_2Ru_2O_7$	0.333	0.323	− 0.010	2
$Eu_2Mo_2O_7$	0.322	0.324	0.002	2
$Sm_2Mo_2O_7$	0.343	0.324	− 0.019	2
$Lu_2Sn_2O_7$	0.340	0.331	− 0.009	8
$Yb_2Sn_2O_7$	0.339	0.330	− 0.009	8
$Er_2Sn_2O_7$	0.338	0.329	− 0.009	8
$Y_2Sn_2O_7$	0.337	0.329	− 0.008	8
$Gd_2Sn_2O_7$	0.335	0.327	− 0.008	8
$Eu_2Sn_2O_7$	0.334	0.327	− 0.007	8
$Sm_2Sn_2O_7$	0.333	0.326	− 0.007	8
$Nd_2Sn_2O_7$	0.332	0.326	− 0.006	8
$Pr_2Sn_2O_7$	0.331	0.325	− 0.006	8
$La_2Sn_2O_7$	0.329	0.324	− 0.005	8
$Eu_2Zr_2O_7$	0.334	0.329	− 0.005	2
$Sm_2Zr_2O_7$	0.342	0.329	− 0.013	This study
$Pr_2Zr_2O_7$	0.335	0.327	− 0.008	This study
$La_2Zr_2O_7$	0.333	0.326	− 0.007	This study
$Eu_2Pb_2O_7$	0.345	0.331	− 0.014	2

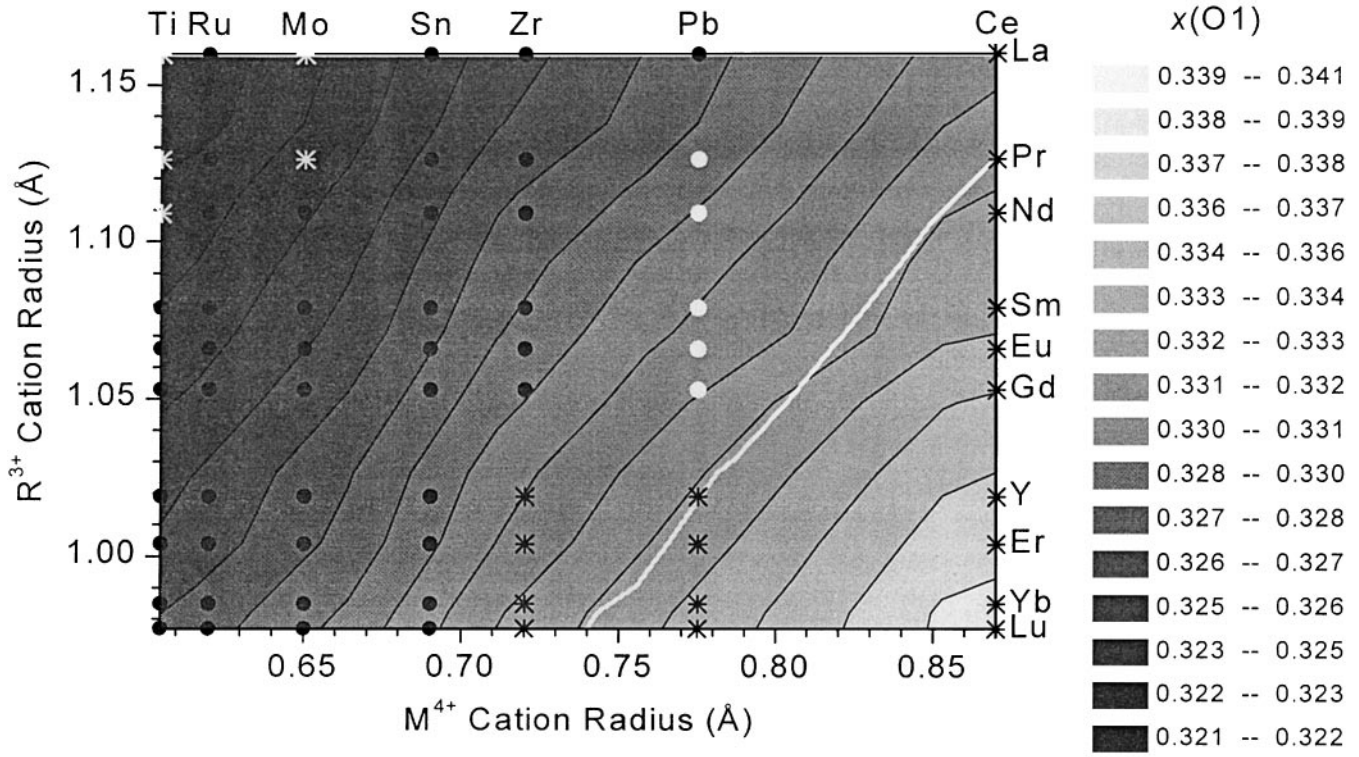

FIG. 10. Contour map of the predicted x values for pyrochlores with various combinatons of R^{3+} and M^{4+} cations.

disorder making the usual assumption of no cation anti-site disorder for the $\varepsilon = 0.50$ specimen) relative to the value of 0.342 for $\varepsilon = 0.50$. The very existence of a wide-range non-stoichiometric solid solution ($0.38 < \varepsilon < 0.55$) in this system shows that cation anti-site disorder must be entropically stabilized at the (necessarily) relatively high temperatures of synthesis. A systematic underestimation of x of ~ 0.007 would therefore seem to imply a level of at least 10% cation anti-site disorder.

The same idea can also be used to rationalize differences in theoretical as compared with experimental rates of change of the predicted x values with rare earth R^{3+} ion size for the same M^{4+} cation. In the case of the stannate pyrochlores (see Table 2) the value of Δ, the difference between experimental and predicted x value, decreases from Lu to La, that is, as a function of R^{3+} cation radius. This is consistent with a systematic decrease in cation site disorder from Lu to La. A recent study of disorder in pyrochlore oxides using the same computer simulation technique likewise concluded that disorder enthalpies decrease with increasing R^{3+} cation size. The increase in disorder with increasing M^{4+} cation radius is predicted to be even more dramatic, in which case one would expect the greatest amount of disorder for the zirconate pyrochlores followed by the stannate pyrochlores with the least amount of disorder for the titanate pyrochlores (13). This would explain why, in the case of the zirconate pyrochlores, the predicted difference in x value from the $R = \text{La}$ to $R = \text{Sm}$ compound is much less than the observed value of ~ 0.10 since the $R = \text{Sm}$ compound has a rather higher degree of cation disorder than the $R = \text{La}$ compound. Given that the composition width of the pyrochlore solid solution field in the $(1 - \varepsilon)ZrO_2 \cdot \varepsilon LaO_{1.5}$ system (for specimens rapidly quenched from 1500°C) is rather narrow (< 2 mol% in width) whereas the corresponding composition width in the case of the $R = \text{Sm}$ compound is much broader ~ 17–18 mol% (9, 20), this would seem to be a reasonable assumption.

6. CONCLUSIONS

Through a combination of experimental and computer modeling techniques it has proved possible, in general trend terms, to establish how the oxygen atom positional parameter, x, varies systematically as a function of R^{3+} and M^{4+} cation radius over an extensive range of $R_2M_2O_7$ oxide pyrochlores. Furthermore this study provides data not only for materials which have already been synthesized but also for compounds which have yet to be synthesized. The experimental studies have determined new x values for $La_2Zr_2O_7$, $Pr_2Zr_2O_7$, $Sm_2Zr_2O_7$, $Sm_2Ti_2O_7$, $Gd_2Ti_2O_7$, and $Er_2Ti_2O_7$. A systematic variation in x as a function of R^{3+} cation radius for both the zirconate and titanate

pyrochlores has been found (see Fig. 2). The previously reported X-ray determined value for x in the case of $Gd_2Ti_2O_7$ was found to be too small. The predicted variation is in good agreement with experimental data (see Table 2). Deviations from prediction suggest the presence of cation anti-site disorder. This study is important in that it demonstrates how a computational method can be used to underpin and perhaps extend the results of complex and difficult experiments since systematic variations can be shown to be reliable even when absolute values exhibit a small constant shift.

ACKNOWLEDGMENTS

Support for the theoretical part of this work was provided by the Department of Energy, Office of Basic Sciences, Division of Materials Sciences. Some computing facilities were provided by EPSRC Grant GR/L86821. One of the authors (Y.T.) gratefully acknowledges the award of an Australian Research Council Post-doctoral Fellowship.

REFERENCES

1. M. A. Subramanian and A. W. Sleight, *in* "Handbook on the Physics and Chemistry of the Rare Earths" (K. A. Gschneidner, Jr., and L. Eyring, eds.) Vol. **16,** Chap. 107, 225–248 (1993).
2. M. A. Subramanian, G. Aravamudan, and G.V. Subba Rao, *Prog. Solid. State Chem.* **15,** 55 (1983).
3. Y. Tabira and R. L. Withers, *Phil. Mag. A* **79,** 1335 (1999).
4. C. R. A. Catlow and W. C. Mackrodt (eds.), "Computer Simulation of Solids" Springer-Verlag, Berlin, 1982.
5. A. H. Harker and R. W. Grimes (Eds.), *in* "Molecular Simulation" (A. H. Harker and R. W. Grimes, Eds.), Vols. 4 and 5 (1990).
6. C. R. A. Catlow, R. G. Bell and J. D. Gale, *J. Mater. Chem.* **4**(6), 781 (1994).
7. O. Knop, F. Brisse, and L. Castelliz, *Can. J. Chem.* **47,** 971 (1969).
8. B. J. Kennedy, B. A. Hunter, and C. J. Howard, *J. Solid State Chem.* **130,** 58 (1997).
9. Y. Tabira and R. L. Withers, *J. Solid State Chem.* **148,** 205 (1999).
10. R. D. Shannon, *Acta Crystallogr. B* **32,** 751 (1976).
11. D. M. Bird and Q.A. King, *Acta Crystallogr. A* **46,** 202 (1990).
12. P. P. Ewald, *Ann. Phys.* **64,** 253 (1921).
13. L. Minervini, R. W. Grimes, and K. E. Sickafus, submitted for publication (1999).
14. B. G. Dick and A.W. Overhauser, *Phys. Rev.* **112,** 90 (1958).
15. M. Leslie, "DL/SCI/TM31T," Technical Report. SERC Daresbury Laboratory, Daresbury, UK, 1982.
16. D. Altermatt and I. D. Brown, *Acta Crystallogr. B* **41,** 240 (1985).
17. N. E. Brese and M. O'Keeffe, *Acta Crystallogr. B* **47,** 192 (1991).
18. I. D. Brown, *Acta Crystallogr. B* **33,** 1305 (1977).
19. Y. Tabira, R. Withers, J. G. Thompson, and S. Schmid, *J. Solid State Chem.* **142,** 393 (1999).
20. A. W. Sleight, *Inorg. Chem.* **8,** 1807 (1969).
21. L. Minervini, M. O. Zacate, and R. W. Grimes, *Solid State Ionics* **116,** 339 (1999).
22. B. J. Kennedy, *Acta Crystallogr. C* **51,** 790 (1995)